ADAPTIVE DUAL SYNCHRONIZATION OF CHAOTIC (HYPERCHAOTIC) COMPLEX SYSTEMS WITH UNCERTAIN PARAMETERS AND ITS APPLICATION IN IMAGE ENCRYPTION

Gamal M. Mahmoud, Ahmed A. Farghaly
Tarek M. Abed-Elhameed, Mohamed M. Darwish

Department of Mathematics, Faculty of Science, Assiut University
Assiut 71516, Egypt

(Received March 27, 2018; accepted August 20, 2018)

The adaptive dual synchronization of chaotic (hyperchaotic) complex systems with uncertain parameters has been investigated. The analytical control functions are derived using a theorem to synchronize the chaotic (hyperchaotic) solutions of these systems. The adaptive dual synchronization between the chaotic complex Chen and Lorenz systems is introduced as an example, and another example is used to test the validity of the technique of this paper. Other examples of chaotic or hyperchaotic complex systems can be similarly studied. Based on the up-to-date laws, the parameters of the drive systems can be identified. The image encryption technique based on the adaptive dual synchronization of chaotic complex Chen and Lorenz systems is presented for gray and color images in the same time. Meantime, in the receiver side, information can be recovered successfully by adaptive technique. The presented technique is robust with respect to different levels of white Gaussian noise. The communication channel as well as the effect of the increase of noise are big challenge which have not been considered. Numerical simulations are given to verify the feasibility of our proposed synchronization and better performance of image encryption technique in terms of histogram, robustness to noise and visual imperceptibility.

DOI:10.5506/APhysPolB.49.1923

1. Introduction

Chaotic systems play an important role in dynamical systems due to their interesting and complex dynamical behaviors. The chaotic system is a three- or higher dimensional system, which has one positive Lyapunov exponent, and has more complex and rich dynamics. The chaotic systems may be important in some sciences such as information processing, computing, telecommunications and electrical engineering [1–4]. Several chaotic

systems have been studied, such as chaotic Rössler, Lü, Lorenz, Chua and Chen systems [5–9]. Mahmoud *et al.* studied the chaotic complex Chen, Lü and Lorenz systems in [10, 11].

In the last four decades, chaos synchronization has became a hot research topic. Synchronization between chaotic systems is more secure than chaotic ones. Synchronization techniques have great potential for applications in several fields such as physics, biological models, engineering applications, secure communication, image encryption and neural networks [12–19]. There exist many types of control to achieve synchronization such as active control, nonlinear feedback control, adaptive control, tracking control, delay feedback control and open-plus-closed-loop control [20–29].

With the rapid growth of the Internet and wireless networks, information security becomes more and more important and it is a critical issue. In particular, image encryption has received a great deal of increasing interest, due to the fact that most of image data are required to be confidential between the sending side and the receiver end, such as some military images, architectural drawings, medical imaging, and so on. During the last several decades, numerous encryption algorithms have been proposed in the literature based on different principles [30–32]. Among them, chaos-based encryption techniques is considered good for practical applications as these techniques provide a good combination of speed, high security, high sensitivity, complexity, *etc.*

The main aim of this paper is to synchronize two chaotic complex systems with uncertain parameters as the adaptive dual synchronization. Based on adaptive dual synchronization, we propose an image encryption algorithm for both gray and color images at the same time.

This paper is organized as follows. In Section 2, the adaptive dual synchronization (ADS) of chaotic complex systems with uncertain parameters is studied. In Section 3, the ADS for chaotic complex Chen and Lorenz systems is stated as an example. Another example is used to test the validity of the technique of this paper using the hyperchaotic complex Lü and Liu systems. The image encryption algorithm is given based on our presented synchronization in Section 4. The availability of the proposed technique is verified by numerical simulations. Different levels of white Gaussian noise are used to evaluate the robustness of the presented scheme. Finally, conclusions are given in Section 5.

2. ADS for chaotic complex systems

In this section, we extend the scheme of ADS of chaotic real systems [33] to chaotic (hyperchaotic) complex systems with uncertain parameters. We require one pair of two chaotic (hyperchaotic) complex systems for the drive system and other pair for the response system. Let the drive systems be

described as

$$\dot{x_1}(t) = F^1(x_1(t))A_1 + f_1(x_1)\,, \tag{1}$$
$$\dot{x_2}(t) = F^2(x_2(t))A_2 + f_2(x_2)\,, \tag{2}$$

where $x_1 \in \boldsymbol{C^n}$, $x_2 \in \boldsymbol{C^m}$, the matrices $F^1 \in \boldsymbol{C^{n\times p_1}}$ and $F^2 \in \boldsymbol{C^{m\times p_2}}$, and the vectors $A_1 \in \boldsymbol{C^{p_1}}$, $A_2 \in \boldsymbol{C^{p_2}}$, $f_1(x_1) \in \boldsymbol{C^n}$ and $f_2(x_2) \in \boldsymbol{C^m}$. We can write systems (1)–(2) as

$$\dot{x}(t) = F(x(t))A + f(x)\,, \tag{3}$$

where 'T' stands for transpose

$$x = (x_1, x_2)^{\mathrm{T}}\,, \qquad A = (A_1, A_2)^{\mathrm{T}}\,, \qquad f(x) = (f_1(x_1), f_2(x_2))^{\mathrm{T}}$$

and

$$F(x) = \begin{pmatrix} F^1(x_1) & 0 \\ 0 & F^2(x_2) \end{pmatrix}.$$

The response systems are given as

$$\dot{y_1}(t) = F^1(y_1(t))\hat{A}_1 + f_1(y_1) + u\,, \tag{4}$$
$$\dot{y_2}(t) = F^2(y_2(t))\hat{A}_2 + f_2(y_2) + v\,, \tag{5}$$

where $y_1 \in \boldsymbol{C^n}$, $y_2 \in \boldsymbol{C^m}$, $\hat{A}_1 \in \boldsymbol{C^{p_1}}$, $\hat{A}_2 \in \boldsymbol{C^{p_2}}$ represent the estimate vectors of A_1 and A_2. $u : \boldsymbol{C^n} \times \boldsymbol{C^n} \longrightarrow \boldsymbol{C^n}$ and $v : \boldsymbol{C^m} \times \boldsymbol{C^m} \longrightarrow \boldsymbol{C^m}$ are two vectors of control functions for the response systems (4)–(5). Systems (4)–(5) can be written as

$$\dot{y}(t) = F(y(t))\hat{A} + f(y) + U\,, \tag{6}$$

where

$$y = (y_1, y_2)^{\mathrm{T}}\,, \quad \hat{A} = \left(\hat{A}_1, \hat{A}_2\right)^{\mathrm{T}}\,, \quad f(y) = (f_1(y_1), f_2(y_2))^{\mathrm{T}}\,, \quad U = (u, v)^{\mathrm{T}}$$

and

$$F(y) = \begin{pmatrix} F^1(y_1) & 0 \\ 0 & F^2(y_2) \end{pmatrix}.$$

Definition 1 *The drive system (3) is said to be dual synchronization with the response system (6), if*

$$\lim_{t\to\infty} \|e\| = \lim_{t\to\infty} \|y - x\| = 0\,. \tag{7}$$

Remark 1 *The error signal of dual synchronization can be written as*

$$e = \begin{bmatrix} e_1 \\ e_2 \end{bmatrix} = \begin{bmatrix} y_1 - x_1 \\ y_2 - x_2 \end{bmatrix} . \tag{8}$$

Remark 2 *If either $x_1 = y_1 = 0$ or $x_2 = y_2 = 0$, then dual synchronization becomes a complete synchronization between two chaotic complex systems.*

The error dynamical system of synchronization can be written as

$$\dot{e} = \dot{y} - \dot{x} . \tag{9}$$

From systems (3) and (6), system (9) can be written as

$$\dot{e} = f(y) - f(x) + (F(y) - F(x))A + F(y)e_A + U , \tag{10}$$

where $e_A = \hat{A} - A$.

Theorem 1 *The drive system (3) and the response system (6) can achieve ADS if the vector of control functions is chosen as follows:*

$$U = f(x) - f(y) + (F(x) - F(y))A - Ke , \tag{11}$$

and the estimated parameters updating the law are selected as

$$\dot{e}_A = \dot{\hat{A}} = -(F(y))^H e , \tag{12}$$

where $K = \mathrm{diag}(k_1, k_2, \ldots, k_{n+m})$ is diagonal gain matrix.

Proof: Let the Lyapunov function be selected as

$$V = \tfrac{1}{2} \left(e^H e + e_A^H e_A \right) , \tag{13}$$

the time derivative of V can be written as

$$\dot{V} = \tfrac{1}{2} \left(e^H \dot{e} + \dot{e}^H e + e_A^H \dot{e}_A + \dot{e}_A^H e_A \right) , \tag{14}$$

and using Eqs. (10)–(12), Eq. (14) takes the form of

$$\begin{aligned} \dot{V} &= -e^H K e \\ &\leq -k_{\min} \|e\|^2 , \end{aligned} \tag{15}$$

where $k_{\min} = \min(k_1, k_2, \ldots, k_{n+m})$. Based on the Lyapunov stability theorem, since V is positive definite and $\dot{V}$ is negative definite, the drive system (3) and the response system (6) achieve the ADS. □

3. Illustrative examples

In this section, we will test our synchronization scheme with two examples. the first one by taking a pair of chaotic complex Chen and Lorenz systems and the other example for hyperchaotic complex Lü and Liu systems [34, 35].

3.1. Example 1

We consider that the chaotic complex Chen and Lorenz systems are the drive systems, respectively,

$$\begin{aligned}
\dot{x}_{11} &= a_1(x_{12} - x_{11})\,, \\
\dot{x}_{12} &= a_4 x_{11} + a_3 x_{12} - x_{11}x_{13}\,, \\
\dot{x}_{13} &= \tfrac{1}{2}(x_{11}\bar{x}_{12} + \bar{x}_{11}x_{12}) - a_2 x_{13}\,, \qquad (16)\\
\dot{x}_{21} &= b_1(x_{22} - x_{21})\,, \\
\dot{x}_{22} &= b_3 x_{21} - x_{22} - x_{21}x_{23}\,, \\
\dot{x}_{23} &= \tfrac{1}{2}(x_{21}\bar{x}_{22} + \bar{x}_{21}x_{22}) - b_2 x_{23}\,, \qquad (17)
\end{aligned}$$

where $x_{11} = x_{11}^r + jx_{11}^i$, $x_{12} = x_{12}^r + jx_{12}^i$, $x_{13} = x_{13}^r$, $x_{21} = x_{21}^r + jx_{21}^i$, $x_{22} = x_{22}^r + jx_{22}^i$, and $x_{23} = x_{23}^r$. If $a_1 = 35$, $a_2 = 3$, $a_3 = 12$, $a_4 = 7$, $b_1 = 12$, $b_2 = 30$, $b_3 = 3$, and the initial conditions of systems (16)–(17) are $x_{10} = x_{20} = (9.4735 + 9.4735j, 10.4211 + 10.4211j, 19.5689)^{\mathrm{T}}$, then these systems have chaotic solutions [10, 11] which are shown in Fig. 1.

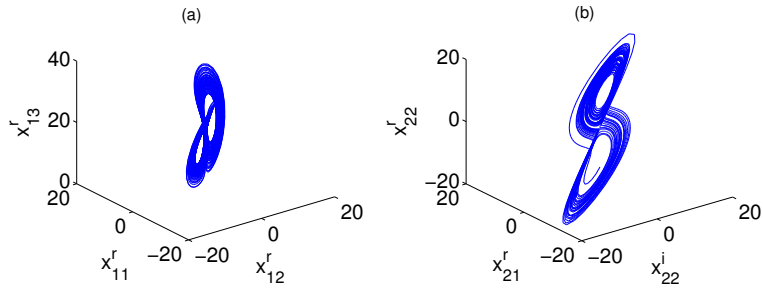


Fig. 1. Chaotic attractors of: (a) system (16) in $x_{12}^r, x_{11}^r, x_{13}^r$ space, (b) system (17) in $x_{22}^i, x_{21}^r, x_{22}^r$ space.

We can write the two drive systems (16)–(17) in the form of Eq. (3) such that: $x = (x_{11}, x_{12}, x_{13}, x_{21}, x_{22}, x_{23})^{\mathrm{T}}$, $f(x) = [0, -x_{11}x_{13}, 0.5(x_{11}\bar{x}_{12} + \bar{x}_{11}x_{12}), 0, -x_{22} - x_{21}x_{23}, 0.5(x_{21}\bar{x}_{22} + \bar{x}_{21}x_{22})]^{\mathrm{T}}$, $A = (a_1, a_2, a_3, a_4, b_1, b_2, b_3)^{\mathrm{T}}$,

and

$$F(x(t)) = \begin{pmatrix} (x_{12}-x_{11}) & 0 & 0 & 0 & 0 & 0 & 0 \\ 0 & 0 & x_{12} & x_{11} & 0 & 0 & 0 \\ 0 & -x_{13} & 0 & 0 & 0 & 0 & 0 \\ 0 & 0 & 0 & 0 & (x_{22}-x_{21}) & 0 & 0 \\ 0 & 0 & 0 & 0 & 0 & 0 & x_{21} \\ 0 & 0 & 0 & 0 & 0 & -x_{23} & 0 \end{pmatrix}.$$

In similar way, we can write the corresponding two response systems as

$$\begin{aligned} \dot{y}_{11} &= \hat{a}_1(y_{12}-y_{11}) + u_1\,, \\ \dot{y}_{12} &= \hat{a}_4 y_{11} + \hat{a}_3 y_{12} - y_{11}y_{13} + u_2\,, \\ \dot{y}_{13} &= \tfrac{1}{2}(y_{11}\bar{y}_{12} + \bar{y}_{11}y_{12}) - \hat{a}_2 y_{13} + u_3\,, \end{aligned} \tag{18}$$

$$\begin{aligned} \dot{y}_{21} &= \hat{b}_1(y_{22}-y_{21}) + v_1\,, \\ \dot{y}_{22} &= \hat{b}_3 y_{21} - y_{22} - y_{21}y_{23} + v_2\,, \\ \dot{y}_{23} &= \tfrac{1}{2}(y_{21}\bar{y}_{22} + \bar{y}_{21}y_{22}) - \hat{b}_2 y_{23} + v_3\,. \end{aligned} \tag{19}$$

The response systems (18)–(19) can be written in the form of Eq. (6), where $\hat{A} = (\hat{a}_1, \hat{a}_2, \hat{a}_3, \hat{a}_4, \hat{b}_1, \hat{b}_2, \hat{b}_3)^{\mathrm{T}}$, $U = (u_1, u_2, u_3, v_1, v_2, v_3)$.

In the numerical simulation, we consider the same parameters and initial conditions of the drive systems (16)–(17) of Fig. 1, and for response systems (18)–(19), $y_{10} = y_{20} = (9.4735 + 9.4735j, 10.4211 + 10.4211j, 19.5689)^{\mathrm{T}}$ and the unknown parameters are chosen also the same as in Fig. 1. By applying Theorem 1, the control functions (11) can be written as

$$U = \begin{pmatrix} 35(x_{12}-x_{11}-y_{12}+y_{11}) - k_1e_{11} \\ y_{11}y_{31} - x_{11}x_{13} + 12(x_{12}-y_{12}) + 7(x_{11}-y_{11}) - k_2e_{12} \\ 0.5(x_{11}\bar{x}_{12} + \bar{x}_{11}x_{12}) - 0.5(y_{11}\bar{y}_{12} + \bar{y}_{11}y_{12}) + 3(y_{13}-x_{13}) - k_3e_{13} \\ 12(x_{22}-x_{21}-y_{22}+y_{21}) - k_4e_{21} \\ y_{22} + y_{21}y_{23} - x_{22} - x_{21}x_{23} + 3(x_{21}-y_{21}) - k_5e_{22} \\ 0.5(x_{21}\bar{x}_{22} + \bar{x}_{21}x_{22}) - 0.5(y_{21}\bar{y}_{22} + \bar{y}_{21}y_{22}) + 30(y_{23}-x_{23}) - k_6e_{23} \end{pmatrix}, \tag{20}$$

where $K = \mathrm{diag}(k_1, k_2, \ldots, k_6) = \mathrm{diag}(5, 6, 7, 3, 4, 2)$ and $e = (e_{11}, e_{12}, e_{13}, e_{21}, e_{22}, e_{23})^{\mathrm{T}} = (e^r_{11} + je^i_{11}, e^r_{12} + je^i_{12}, e^r_{13}, e^r_{21} + je^i_{21}, e^r_{22} + je^i_{22}, e^r_{23})^{\mathrm{T}}$. The results are shown in Figs. 2–5. Figures 2–3 show that the ADS errors approach zero, while in Figs. 4–5, the estimate of unknown parameters $\hat{A} = (\hat{a}_1, \hat{a}_2, \hat{a}_3, \hat{a}_4, \hat{b}_1, \hat{b}_2, \hat{b}_3)^{\mathrm{T}}$ converge to $A = (a_1, a_2, a_3, a_4, b_1, b_2, b_3)^{\mathrm{T}} = (35, 3, 12, 7, 12, 30, 3)^{\mathrm{T}}$.

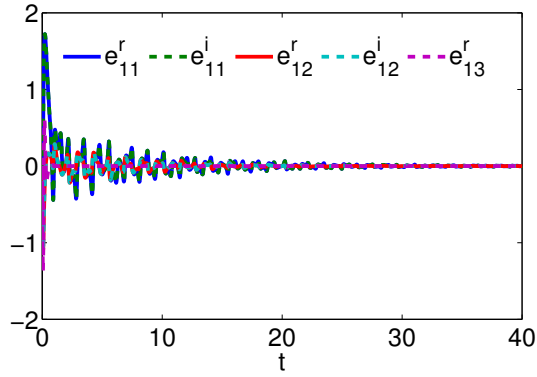


Fig. 2. Synchronization errors for the drive system (16) and the response system (18) *versus* t.

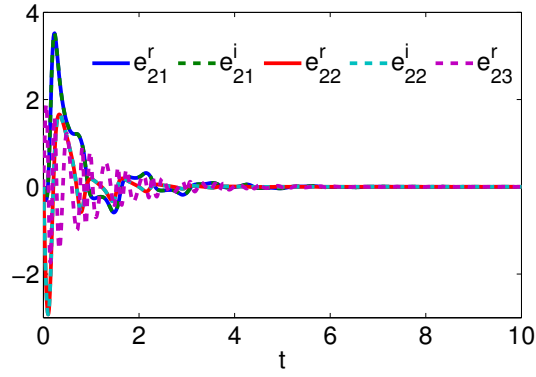


Fig. 3. Synchronization errors for the drive system (17) and the response system (19) *versus* t.

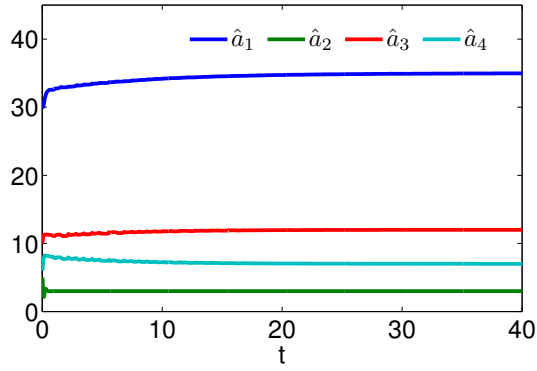


Fig. 4. Parameters identified for the drive system (16).

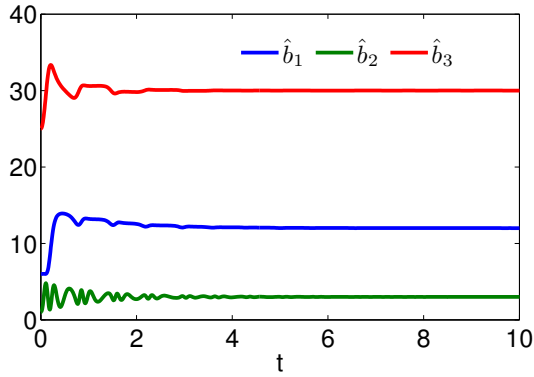


Fig. 5. Parameters identified for the drive system (17).

3.2. Example 2

Now, we will test our scheme with the hyperchaotic complex Lü and Liu systems, which are written as

$$\begin{aligned}
\dot{z}_{11} &= c_1(z_{12} - z_{11}) + z_{14}\,,\\
\dot{z}_{12} &= c_2 z_{12} - z_{11} z_{13} + z_{14}\,,\\
\dot{z}_{13} &= \tfrac{1}{2}(z_{11}\bar{z}_{12} + \bar{z}_{11} z_{12}) - c_3 z_{13}\,,\\
\dot{z}_{14} &= \tfrac{1}{2}(z_{11}\bar{z}_{12} + \bar{z}_{11} z_{12}) - c_4 z_{14}\,, \qquad (21)\\
\dot{z}_{21} &= d_1(z_{22} - z_{21})\,,\\
\dot{z}_{22} &= d_2 z_{21} + z_{21} z_{23} - z_{24}\,,\\
\dot{z}_{23} &= -\tfrac{1}{2}(z_{21}\bar{z}_{22} + \bar{z}_{21} z_{22}) - d_3 z_{23} + z_{24}\,,\\
\dot{z}_{24} &= \tfrac{1}{2} d_4(z_{21} + \bar{z}_{21}) + \tfrac{1}{2}(z_{22} + \bar{z}_{22})\,, \qquad (22)
\end{aligned}$$

where $z_{11} = z_{11}^r + j z_{11}^i$, $z_{12} = z_{12}^r + j z_{12}^i$, $z_{13} = z_{13}^r$, $z_{14} = z_{14}^r$, $z_{21} = z_{21}^r + j z_{21}^i$, $z_{22} = z_{22}^r + j z_{22}^i$, $z_{23} = z_{23}^r$, and $z_{24} = z_{24}^r$. For $c_1 = 42$, $c_2 = 25$, $c_3 = 6$, $c_4 = 5$, $d_1 = 10$, $d_2 = 35$, $d_3 = 1.4$, $d_4 = 5$, and the initial conditions of systems (21)–(22) to be $z_{10} = (-9.7108 - 0.1059j, -8.4210 - 0.0929j, 26.3764, 31.4969)^{\mathrm{T}}$, $z_{20} = (0.6654 + 0.0103j, -24.6381 - 0.2534j, -66.9976, 18.5105)^{\mathrm{T}}$, these systems have hyperchaotic solutions.

In similar way, we apply Theorem 1 between the drive systems (21)–(22) and the corresponding response systems using the proposed technique. Then we obtain the control functions and using numerical simulation, we can see that the errors go to zero. The parameters identified for the drive systems (21)–(22) are shown in Figs. 6–9. These results show that our technique gives good results. Other chaotic (hyperchaotic) complex systems can be similarly investigated.

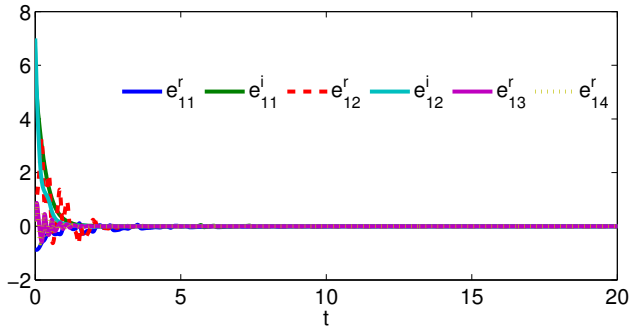


Fig. 6. Synchronization errors for the drive system (21) and the corresponding response system *versus* t.

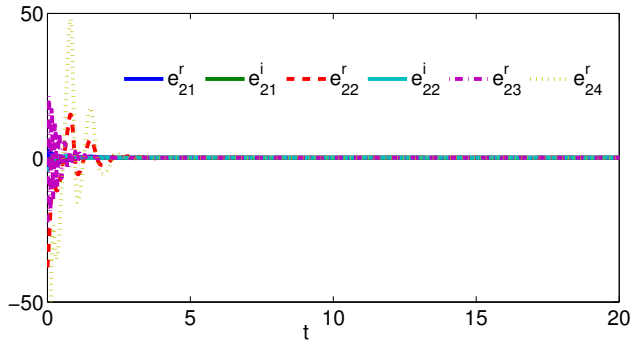


Fig. 7. Synchronization errors for the drive system (22) and the corresponding response system *versus* t.

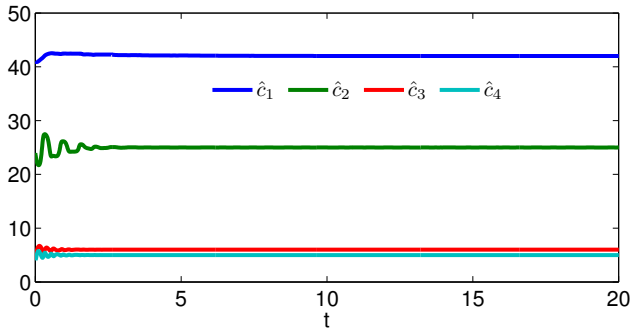


Fig. 8. Parameters identified for the drive system (21).

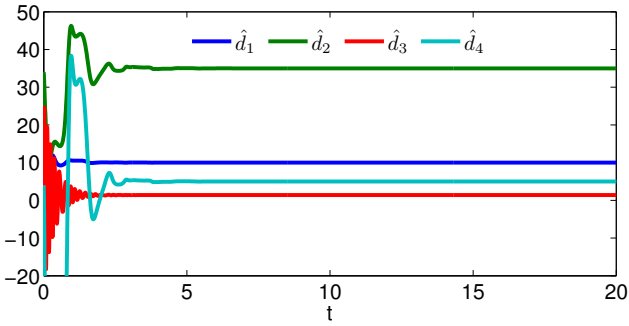


Fig. 9. Parameters identified for the drive system (22).

4. Secure communication

In [17], the adaptive synchronization of chaotic real systems was proposed and the proposed scheme was applied to color image encryption. In our presented scheme, we investigate the adaptive dual synchronization of chaotic complex systems. Based on ADS of chaotic complex systems, we developed image encryption method for gray and color images and the suggested technique is resistant to different levels of noise.

A brief description of secure communication scheme is presented in three subsections. The first one is devoted to secure communication for gray-scale images, while the secure communication for color images is described in the second subsection. The conducted numerical experiments are described in the third subsection.

4.1. Single parameter modulation-based image encryption scheme of grayscale image

The presented scheme of grayscale image based on single parameter modulation is discussed through this subsection. A digital image of the size of $m \times n$, $h(k,l)$ represents the intensity pixel value at the position (k,l), where $k = 1, 2, \ldots, m$, $l = 1, 2, \ldots, n$. The digital signals are modulated by choosing the parameter a_2. The two-dimensional matrix of pixels is transformed into a one-dimensional integer between 0 and 255.

Let the matrix of pixel values of the plain image be given as follows:

$$H = \begin{pmatrix} h_{11} & h_{12} & \ldots & h_{1n} \\ h_{21} & h_{22} & \ldots & h_{2n} \\ \vdots & \vdots & \vdots & \vdots \\ h_{m1} & h_{m2} & \ldots & h_{mn} \end{pmatrix},$$

where m, n represent the image width and high, h_{kl} is the intensity value of image. Let $H = [h_{11}, h_{21}, \ldots, h_{m1}, h_{12}, \ldots, h_{m2}, \ldots, h_{1n}, \ldots, h_{mn}] = [h_1, h_2, \ldots, h_{mn}]$, then each value h_k of H is modulated into the parameter a_2 in the drive system (16) by a function $f(h(r))$, *i.e.*

$$S(t) = g(h(r)) = \frac{h_r}{(10\,d)} + a_2\,, \tag{23}$$

where $r = 1, \ldots, mn$, $d = \max(h(r)) - \min(h(r))$, $a_2 = 3$. The value of $\frac{h_r}{(10\,d)}$ is 0 or 0.1 which means that system (16) maintains the chaotic behavior according to [10].

Moreover, the inverse function $g^{-1}(\bar{S}(t))$ can be obtained by the response system (18) as

$$\bar{h}_r = g^{-1}\left(\bar{S}(t)\right) = 10\,\left(\bar{S}(t) - a_2\right)\,d\,, \tag{24}$$

where $r = 1, \ldots, mn$, $d = \max(h(r)) - \min(h(r))$.

4.2. Multi-parameters modulation-based image encryption scheme of color image

In order to deal with color image, we convert the present color images into three Red, Green and Blue (RGB) channel components by using the RGB channels. The parameters b_1, b_2, b_3 are chosen in the drive system (18) as message carriers to transmit the RGB channels of the plain image using the modulation equations given as

$$\begin{aligned} S_{\mathrm{R}}(t) &= g(h_{\mathrm{R}}(r)) = \frac{h_{\mathrm{R}_r}}{(10\,d_{\mathrm{R}})} + b_1\,, \\ S_{\mathrm{G}}(t) &= g(h_{\mathrm{G}}(r)) = \frac{h_{\mathrm{G}_r}}{(10\,d_{\mathrm{G}})} + b_2\,, \\ S_{\mathrm{B}}(t) &= g(h_{\mathrm{B}}(r)) = \frac{h_{\mathrm{B}_r}}{(10\,d_{\mathrm{B}})} + b_3\,, \end{aligned} \tag{25}$$

where $\frac{h_{\mathrm{R}_r}}{(10\,d_{\mathrm{R}})}$, $\frac{h_{\mathrm{G}_r}}{(10\,d_{\mathrm{G}})}$, $\frac{h_{\mathrm{B}_r}}{(10\,d_{\mathrm{B}})} \in [0, 2.55]$. This means that system (17) maintains the chaotic behavior according to [11].

Meanwhile, the inverse functions of (25) are given by the response system (19) as

$$\begin{aligned} \bar{h}_{\mathrm{R}_r} &= g^{-1}\left(\bar{S}_{\mathrm{R}}(t)\right) = 10\,\left(\bar{S}_{\mathrm{R}}(t) - b_1\right)\,d_{\mathrm{R}}\,, \\ \bar{h}_{\mathrm{G}_r} &= g^{-1}\left(\bar{S}_{\mathrm{G}}(t)\right) = 10\,\left(\bar{S}_{\mathrm{G}}(t) - b_2\right)\,d_{\mathrm{G}}\,, \\ \bar{h}_{\mathrm{B}_r} &= g^{-1}\left(\bar{S}_{\mathrm{B}}(t)\right) = 10\,\left(\bar{S}_{\mathrm{B}}(t) - b_3\right)\,d_{\mathrm{B}}\,, \end{aligned} \tag{26}$$

where $r = 1, \ldots, mn$, $d_{\mathrm{R}} = \max(h_{\mathrm{R}}(r)) - \min(h_{\mathrm{R}}(r))$, $d_{\mathrm{G}} = \max(h_{\mathrm{G}}(r)) - \min(h_{\mathrm{G}}(r))$, $d_{\mathrm{B}} = \max(h_{\mathrm{B}}(r)) - \min(h_{\mathrm{B}}(r))$, $b_1 = 12, b_2 = 30, b_3 = 3$.

4.3. Numerical experiments

In order to analyze and evaluate the performance of the secure communication system, the quality of recovered gray and color images is measured by peek signal-to-noise ratio (PSNR) [36] and the structural similarity image index (SSIM). A set of numerical experiments was performed to demonstrate the efficiency of the image encryption scheme depending on ADS, with gray Boat and color Peper image of the size of (256×256). The original gray image is shown in Fig. 10 (a) and its gray distribution is depicted in Fig. 10 (b). In Fig. 10 (c)–(d), the recovered image and its gray corresponding distribution are illustrated, obtained after using the proposed scheme respectively. As shown in Fig. 10, the recovered image is very similar to the original one. Similarly, the original Peper color image can be reconstructed by the recovered three RGB channels and its RGB corresponding distribution is illustrated in Fig. 11. It is noticed that the recovered color image is very close to the original one.

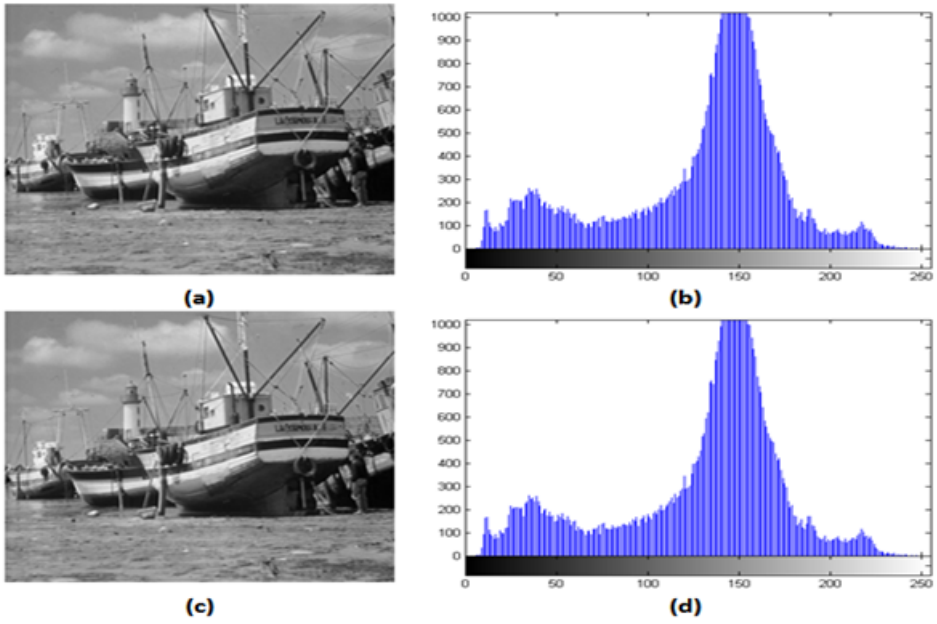


Fig. 10. (a) The original image, (b) the histogram of original image, (c) the recovered image, (d) the histogram of recovered image.

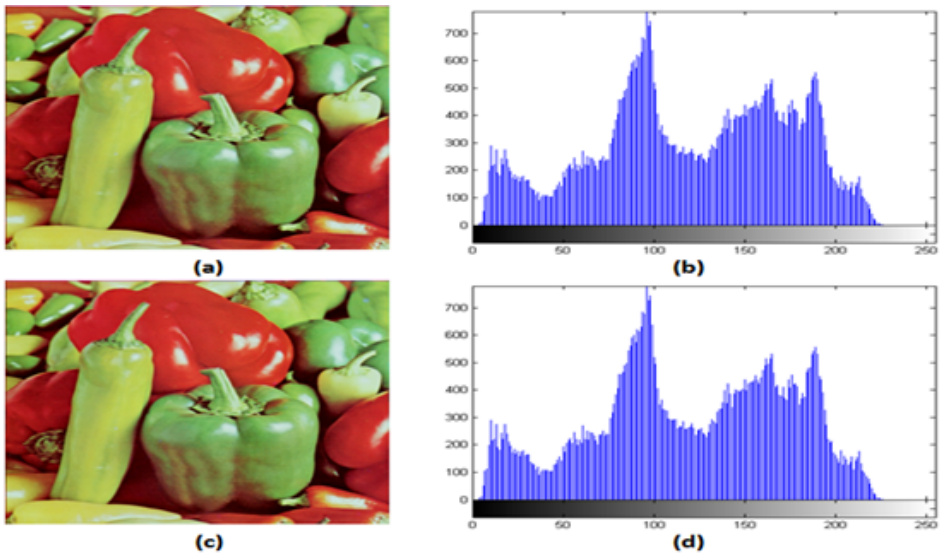


Fig. 11. (a) The original color image, (b) the histogram of original color image, (c) the recovered image, (d) the histogram of recovered image.

4.3.1. Peak signal-to-noise ratio analysis

To verify the decryption quality of the secure communication scheme, the peak signal-to-noise ratio (PSNR) was used to measure the pixel distribution with respect to the original image and a quantitative measure for the recovered image. A PSNR with high values corresponds to a strong similarity between the decrypted image and original ones. The PSNR is defined as follows:

$$\mathrm{PSNR}(h, h_D) = 10 \log_{10} \left[\frac{(255)^2}{\mathrm{MSE}} \right] , \tag{27}$$

where MSE is the mean square error and is defined as

$$\mathrm{MSE} = \frac{1}{m \times n} \sum_{i=1}^{m} \sum_{j=1}^{n} (h_D(i,j) - h(i,j))^2 , \tag{28}$$

and h and h_D represent the original and recovered image, respectively.

4.3.2. The structural similarity index

Another important criteria to evaluate quantitatively the recovered image is the SSIM [37], which is used to measure the similarity between the original and recovered image. The SSIM is defined as follows:

$$\mathrm{SSIM}(h, h_D) = \frac{(2\mu_h\mu_{h_D} + C_1)(2\sigma_{hh_D} + C_2)}{(\mu_h^2 + \mu_{h_D}^2 + C_1)(\sigma_h^2 + \sigma_{h_D}^2 + C_2)}, \tag{29}$$

where μ_h and μ_{h_D} are the average luminance value of original image h and the watermarked image h_D, respectively; σ_h and σ_{h_D} are the standard variance of h and h_D, respectively. σ_{hh_D} is the covariance between h and h_D, C_1 and C_2 are small fixed positive constants adopted to avoid the denominators from being zero. The dynamic range of SSIM is $[-1, 1]$, and the best value 1 is achieved if and only if $h = h_D$. The PSNR and SSIM are calculated for the recovered gray and color image with the original ones, then the corresponding results are listed in Tables I and II.

TABLE I

The PSNR and SSIM values for gray Boat image.

Gray image	PSNR	SSIM
Boat	66.9787	0.9999
Boat Gaussian noise 0.02	66.9787	0.9999
Boat Gaussian noise 0.05	66.9645	0.9999
Boat Gaussian noise 0.1	66.8836	0.9999

TABLE II

The PSNR and SSIM values for color Peper image.

Color image	PSNR	SSIM
Peper	62.9431	0.9999
Peper Gaussian noise 0.02	62.8072	0.9999
Peper Gaussian noise 0.05	62.3304	0.9999
Peper Gaussian noise 0.1	61.4566	0.9999

In order to evaluate the robustness of the proposed scheme to different levels of noise, the noise-free gray and color images of Boat and Peper are used in this experiment, respectively. These gray and color images are contaminated by different levels of the white Gaussian noise, the original and recovered noisy images are displayed in Figs. 10–13, which show that the recovered noisy gray and color images are very similar to the original noisy images.

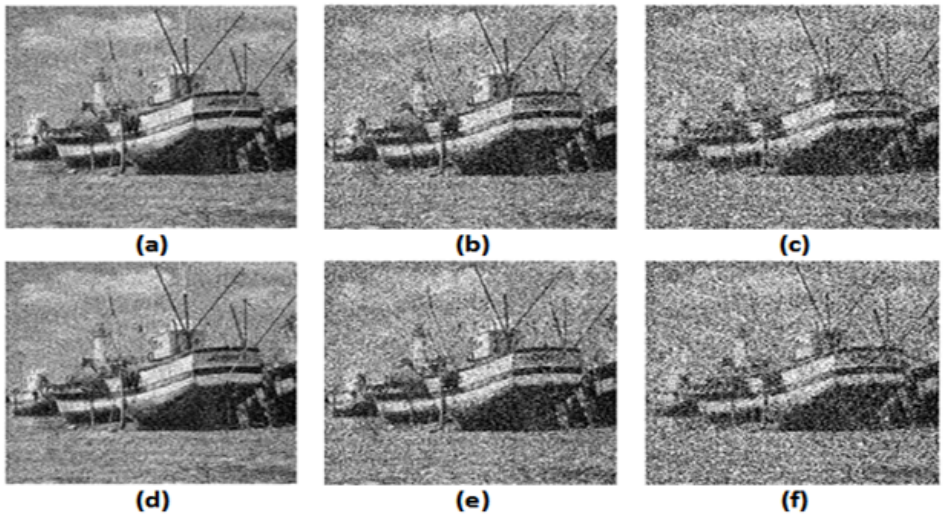


Fig. 12. (a)–(c) The original noisy image with 0.02, 0.05 and 0.1 Gaussian noise, respectively, and (d)–(f) the recovered noisy image with 0.02, 0.05 and 0.1 Gaussian noise, respectively.

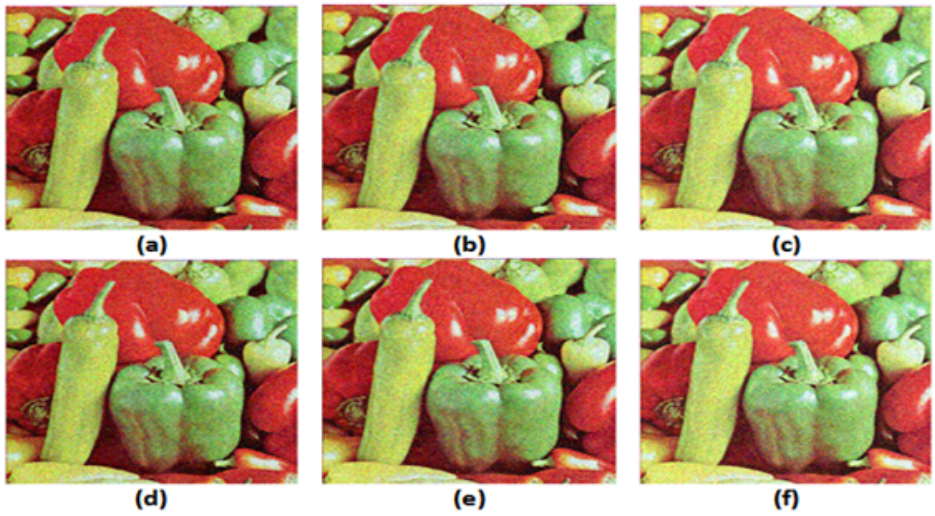


Fig. 13. (a)–(c) The original noisy color image with 0.02, 0.05 and 0.1 Gaussian noise, respectively, and (d)–(f) the recovered noisy image with 0.02, 0.05 and 0.1 Gaussian noise, respectively.

5. Conclusion

The adaptive dual synchronization of chaotic complex systems with uncertain parameters has been investigated. Using the Lyapunov stability theory, analytical formula of control functions (11) has been derived. This type of synchronization has been applied for the chaotic complex Chen and Lorenz systems, and the results are shown in Figs. 2–5. Another example has been stated to test the validity of our technique which is the synchronization of the hyperchaotic complex Lü and Liu systems. By parameter modulation, the chaos-based secure communication scheme has been introduced. The original information signal has been transferred from the parameters of the drive systems (16)–(17) to estimate parameters in the response systems (18)–(19). The transfer information signal has been recovered accurately as shown in Figs. 10 and 11. Experimental results verified the effectiveness of the image encryption technique, robustness to noise and visual imperceptibility.

REFERENCES

[1] J.C. Sprott, *Am. J. Phys.* **68**, 758 (2000).
[2] R. Xu, Q. Gan, Z. Ma, *J. Comput. Appl. Math.* **230**, 187 (2009).
[3] D.V. Efimov, *Int. J. Adapt. Control* **20**, 491 (2006).
[4] Z.M. Ge, G.H. Lin, *Chaos, Solitons Fract.* **34**, 740 (2007).
[5] O.E. Rössler, *Phys. Lett. A* **57**, 397 (1976).
[6] J. Lü, G. Chen, *Int. J. Bifurcat. Chaos* **12**, 659 (2002).
[7] E.N. Lorenz, *J. Atmos. Sci.* **20**, 130 (1963).
[8] V. Belykh, L. Chua, *Int. J. Bifurcat. Chaos* **2**, 697 (1992).
[9] G. Chen, T. Ueta, *Int. J. Bifurcat. Chaos* **9**, 1465 (1999).
[10] G.M. Mahmoud, T. Bountis, E.E. Mahmoud, *Int. J. Bifurcat. Chaos* **17**, 4295 (2007).
[11] G.M. Mahmoud, M.A. Al-Kashif, S.A. Aly, *Int. J. Mod. Phys. C* **18**, 253 (2007).
[12] G.M. Mahmoud, T. Bountis, M. Al-Kashif, S.A. Aly, *Dyn. Syst.* **24**, 63 (2009).
[13] R.E. Mirollo, S.H. Strogatz, *SIAM J. Appl. Math.* **50**, 1645 (1990).
[14] A.C. Luo, *Commun. Nonlinear Sci.* **14**, 1901 (2009).
[15] G.M. Mahmoud, E.E. Mahmoud, A.A. Arafa, *Phys. Scr.* **87**, 055002 (2013).
[16] Y. Xu, H. Wang, Y. Li, B. Pei, *Commun. Nonlinear Sci.* **19**, 3735 (2014).
[17] J. He, J. Cai, J. Lin, *Optik — Int. J. Light Electron Optics* **127**, 2502 (2016).
[18] W. Lu, T. Chen, *IEEE Trans. Circuits Syst. I* **51**, 2491 (2004).

[19] L. Du, Y. Yang, Y. Lei, *Appl. Math. Mech.* **39**, 353 (2018).

[20] M. Daszkiewicz, *Acta Phys. Pol. B* **49**, 1459 (2018).

[21] G.M. Mahmoud, E.E. Mahmoud, A.A. Arafa, *Chaos, Solitons Fract.* **111**, 86 (2018).

[22] G.M. Mahmoud, M.E. Ahmed, T.M. Abed-Elhameed, *Eur. Phys. J. Plus* **131**, 200 (2016).

[23] G.M. Mahmoud, T.M. Abed-Elhameed, A.A. Farghaly, *Chin. Phys. B* **27**, 80502 (2018).

[24] C.J. Wan, D.S. Bernstein, *Dynam. Control* **5**, 321 (1995).

[25] H. Tirandaz, A. Karami-Mollaee, *Acta Phys. Pol. B* **49**, 59 (2018).

[26] X. Wu, J.A. Lu, *Chaos, Solitons Fract.* **22**, 375 (2004).

[27] G.M. Mahmoud, M.E. Ahmed, T.M. Abed-Elhameed, *Optik — Int. J. Light Electron Optics* **130**, 398 (2017).

[28] G.M. Mahmoud, A.A. Arafa, T.M. Abed-Elhameed, E.E. Mahmoud, *Chaos, Solitons Fract.* **104**, 680 (2017).

[29] E.A. Jackson, I. Grosu, *Physica D* **85**, 1 (1995).

[30] G. Chen, Y. Mao, C.K. Chui, *Chaos, Solitons Fract.* **21**, 749 (2004).

[31] N. Pareek, V. Patidar, K. Sud, *Image Vision Comput.* **24**, 926 (2006).

[32] J.C. Yen, J.I. Guo, *IEE Proc. Vision Image Sign.* **147**, 167 (2000).

[33] A.A. Othman, M. Noorani, M.M. Al-Sawalha, *Optik — Int. J. Light Electron Optics* **127**, 7852 (2016).

[34] G.M. Mahmoud, E.E. Mahmoud, M.E. Ahmed, *Nonlinear Dyn.* **58**, 725 (2009).

[35] L. Liu, C.X. Liu, Y.B. Zhang, *Chin. J. Phys.* **46**, 386 (2008).

[36] Z. Wang, A.C. Bovik, *IEEE Sign. Proc. Lett.* **9**, 81 (2002).

[37] Z. Wang, A.C. Bovik, H.R. Sheikh, E.P. Simoncelli, *IEEE Tran. Image Proc.* **13**, 600 (2004).